Absorption Measure Distribution: models vs observations

Agata Różańska[1] Tek P. Adhikari[1] Bożena Czerny[2]
Małgosia Sobolewska[1] Anne-Marie Dumont

[1]N. Copernicus Astronomical Center PAS, Warsaw, Poland
[2]Center for Theoretical Physics PAS, Warsaw, Poland

Chandra Workshop, 19.08.2015

STRONGGRAVITY
EU FP7-SPACE research project 312789 2013 - 2017

POLISH ACADEMY OF SCIENCES
N. COPERNICUS ASTRONOMICAL CENTER

Outline

1. **X-ray absorption in AGN**
   - Observations
   - Spectral analysis
2. **Absorption Measure Distribution**
   - Photoionization calculation
   - AMD

Conclusions
- Summary
- Discussion

Outline

1. **X-ray absorption in AGN**
   - Observations
   - Spectral analysis
2. **Absorption Measure Distribution**
   - Photoionization calculation
   - AMD

Conclusions
- Summary
- Discussion

I will NOT talk about:
1. AGN feedback
2. the wind origin
3. MHD simulations
4. the wind location
5. variability
6. winds in X-ray binaries

First evidence of X-ray absorption – "Warm Absorber"

MR 2252-178 (z=0.064), Halpern 1984, **EINSTEIN HRI**

QSO M

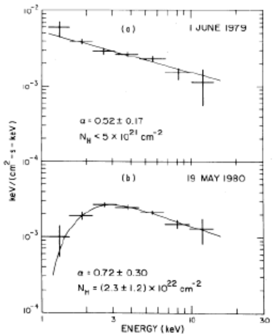

FIG. 1.—*Einstein* MPC spectra for MR 2251−178: (*a*) 1979 June 1; (*b*)

First evidence of X-ray absorption – “Warm Absorber”

MR 2252-178 (z=0.064), Halpern 1984, **EINSTEIN HRI**

QSO M

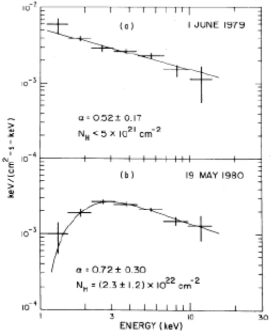

FIG. 1.—*Einstein* MPC spectra for MR 2251−178: (*a*) 1979 June 1; (*b*)

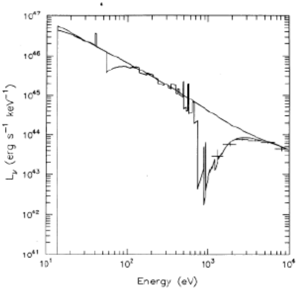

FIG. 3.—Incident and emergent spectra for a shell of column density 6.2×10^{22} and log U = 0, normalized to the MPC spectrum of 1980 May. Prominent absorption edges are due to He II, O VII, and O VIII at 54.4, 739., and 870. eV respectively.

O VII 0.739 keV,
O VIII 0.870 keV

First evidence of X-ray absorption – "Warm Absorber"

MR 2252-178 (z=0.064), Halpern 1984, **EINSTEIN HRI**

QSO M

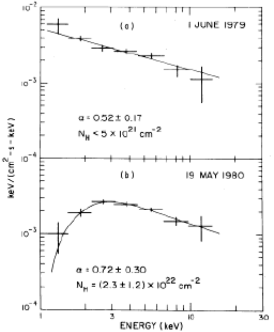

FIG. 1.—*Einstein* MPC spectra for MR 2251−178: (a) 1979 June 1; (b)

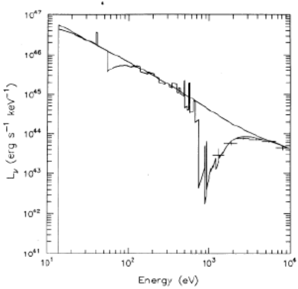

FIG. 3.—Incident and emergent spectra for a shell of column density 6.2×10^{22} and log $U = 0$, normalized to the MPC spectrum of 1980 May. Prominent absorption edges are due to He II, O VII, and O VIII at 54.4, 739., and 870. eV respectively.

OVII 0.739 keV,
OVIII 0.870 keV

Progress of our knowledge about WA is connected with the development of X-ray satellites. **ASCA** (90-ties) - only edges :)

High resolution instrument: CHANDRA

NGC 3783, Sy1, Kaspi + 02
HETG, METG, 900 ksec

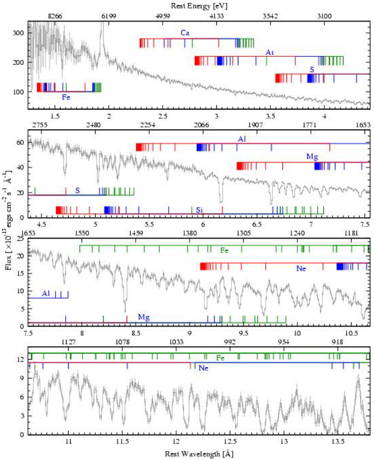

NGC 4051, Sy1, King + 2012
12 HETG, METG, 308 ksec

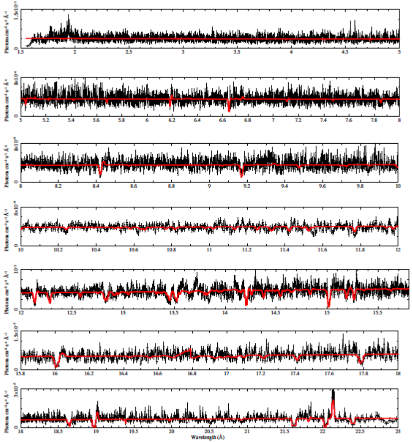

High resolution instrument: XMM-Newton, SUZAKU

NGC 5548, Sy1 Steenbrugge + 03
RGS 137 ksec

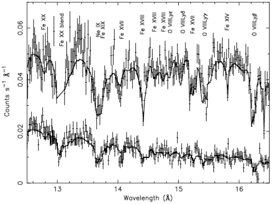

MCG-6-30-15, Miyakawa + 09
SUZAKU

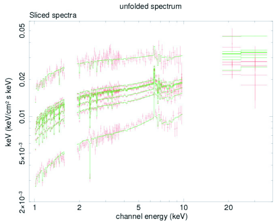

NGC 3516, Sy1 Mehdipour + 10
RGS 260 ksec

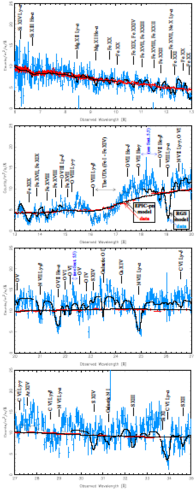

ESO 113-G010, Sy1.8
Mehdipour + 12, RGS 102 ksec

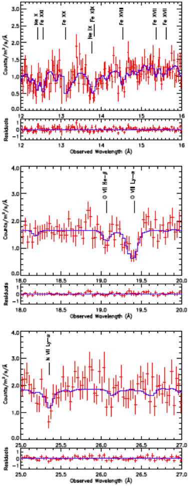

High resolution X-ray spectroscopy

New region of unvisible highly ionized plasma in AGN scheme

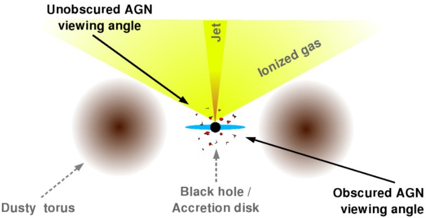

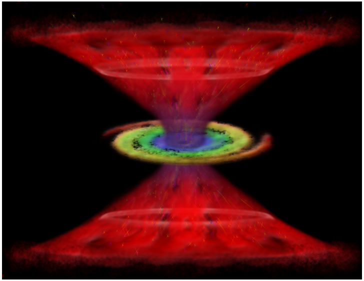

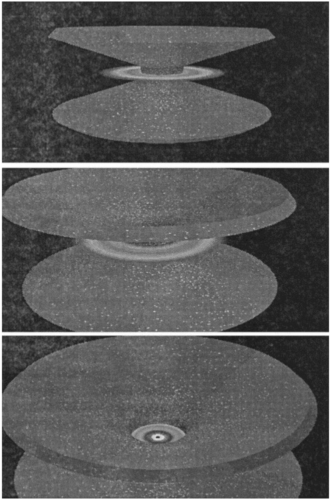

Ionized plasma can be spacially resolved with CHANDRA

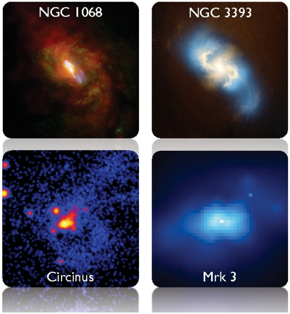

- **NGC 1068 (440 ks)**
  - $N_H > 10^{25}$ cm^{-2} (Evans et al. 2010)
  - HST: Das, Crenshaw & Kraemer (2007)
- **NGC 3393 (350 ks)**
  - Binary BH (Fabbiano et al. 2011)
  - $N_H \sim 2 \times 10^{24}$ cm^{-2} (Fukazawa et al. 2011)
  - HST: Cooke et al. (2000)
- **Circinus (695 ks)**
  - $N_H \sim 2 \times 10^{24}$ cm^{-2} (Yang et al. 2008)
- **Mrk 3 (400 ks)**
  - $N_H \sim 1.1 \times 10^{24}$ cm^{-2} (Awaki et al. 2007)
  - HST: Crenshaw et al. (2010)

Survey of
Outflows in
AGN
Resolved
Spectroscopy

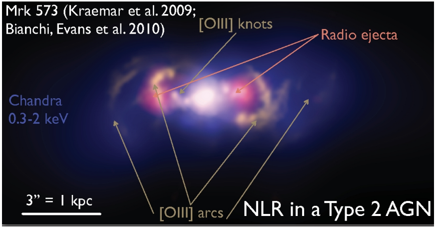

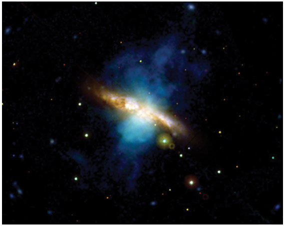

Mrk 509, Detmers + 11
XMM-Newton, RGS 600 ksec

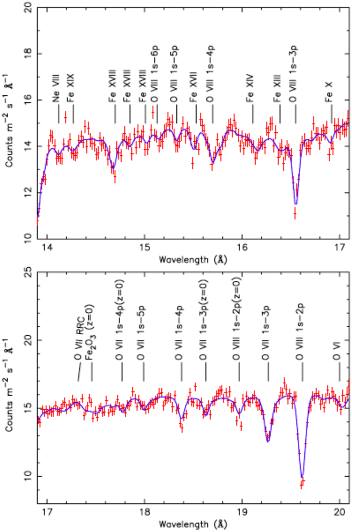

Mrk 509, Detmers + 11
XMM-Newton, RGS 600 ksec

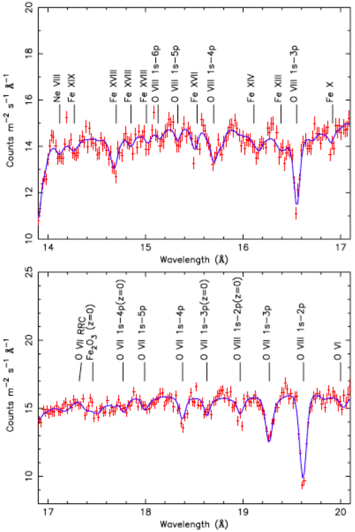

Fitting individual lines

1. each line fitted with Gaussian profile; energy shift gives v_i
2. EW - standard xspec command

Mrk 509, Detmers + 11
XMM-Newton, RGS 600 ksec

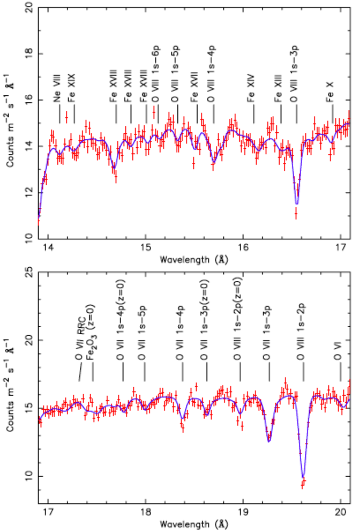

Fitting individual lines

1. each line fitted with Gaussian profile; energy shift gives v_i
2. EW - standard xspec command
3. ionic column densities by integration over model

$$N_i = \frac{m_e c}{\pi e^2 f_i \lambda_i} \int \tau(\nu) d\nu$$

Mrk 509, Detmers + 11
XMM-Newton, RGS 600 ksec

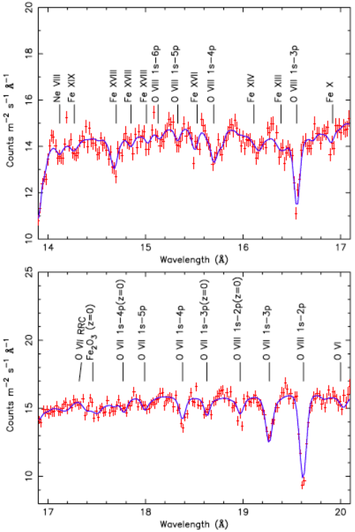

Fitting individual lines

1. each line fitted with Gaussian profile; energy shift gives v_i
2. EW - standard xspec command
3. ionic column densities by integration over model

$$N_i = \frac{m_e c}{\pi e^2 f_i \lambda_i} \int \tau(\nu) d\nu$$

4. with Solar :) abundances photoionization modelling
5. connects N_i with N_H and N_{tot} column denisity of the absorber

Theoretical curve of growth

Linear dependence of EW (named W here) on ionic column density is valid only if lines are unsaturated

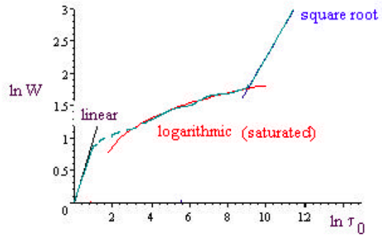

For saturated lines velocity matters

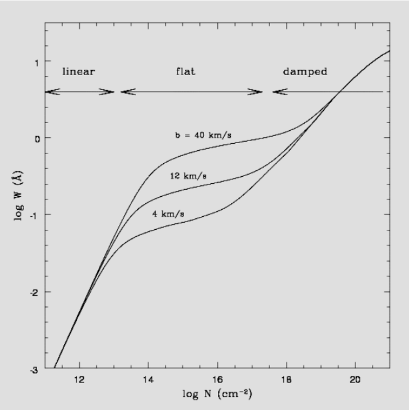

SDSS J0318-0600, Dunn + 10 , VLT, z=1.96

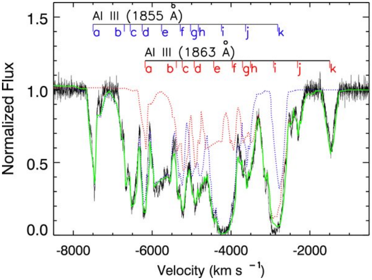

NGC 3783, Holczer + 05, HETG

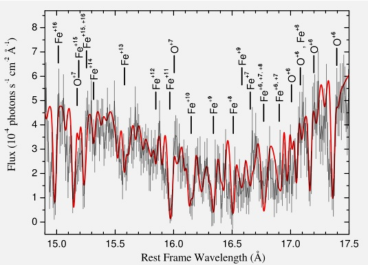

SDSS J0318-0600, Dunn + 10 , VLT, z=1.96

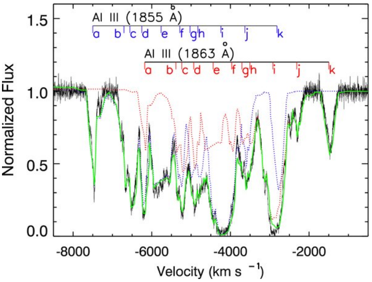

NGC 3783, Holczer + 05, HETG

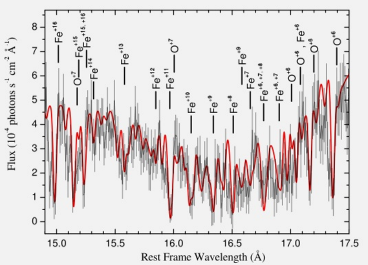

Fitting individual lines in UV

1. lines possess many velocity components
2. different absorbers

SDSS J0318-0600, Dunn + 10 , VLT, z=1.96

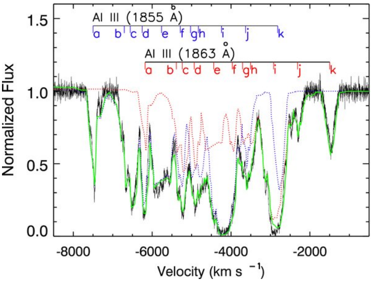

NGC 3783, Holczer + 05, HETG

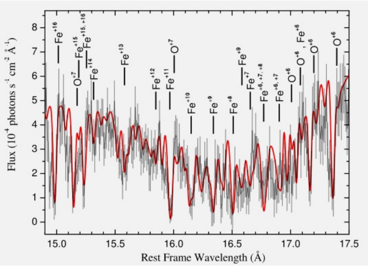

Fitting individual lines in UV

1. lines possess many velocity components
2. different absorbers
3. ionic column densities by integration over data

$$N_i = \frac{m_e c}{\pi e^2 f_i \lambda_i} \int \tau(\nu) d\nu$$

SDSS J0318-0600, Dunn + 10 , VLT, z=1.96

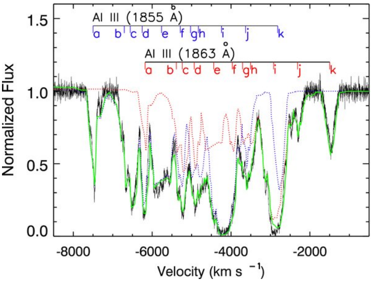

NGC 3783, Holczer + 05, HETG

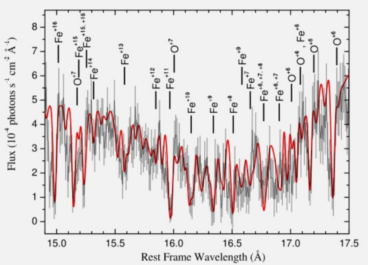

Fitting individual lines in UV

1. lines possess many velocity components
2. different absorbers
3. ionic column densities by integration over data

$$N_i = \frac{m_e c}{\pi e^2 f_i \lambda_i} \int \tau(\nu) d\nu$$

4. covering factor can be obtained

$$\tau_\nu = -ln \left(\frac{I_\nu - 1 - C_f}{C_f} \right)$$

5. photoionization modelling !?

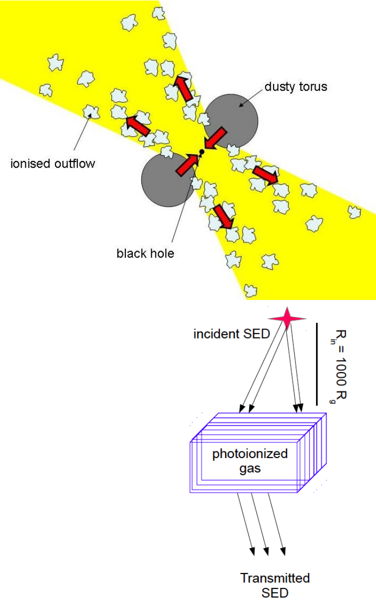
dusty torus
ionised outflow
black hole
incident SED
$R_{in} = 1000\,R_g$
photoionized gas
Transmitted SED

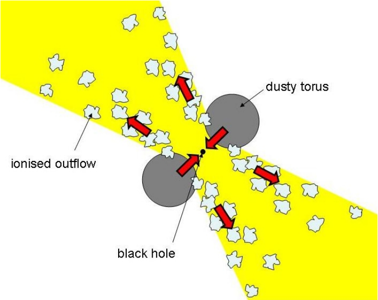

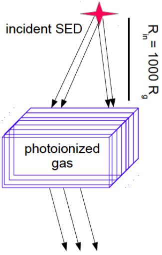

One photoionization component

1. parameters: A_i - Solar :), $R, n_0, N_{tot}, L_{ion}, SED, C_f = 1$
2. 1D non-LTE radiative transfer with ionization and thermal eq.: CLOUDY, XSTAR, TITAN, ION, PHASE, SPEX, XABS, SLAB

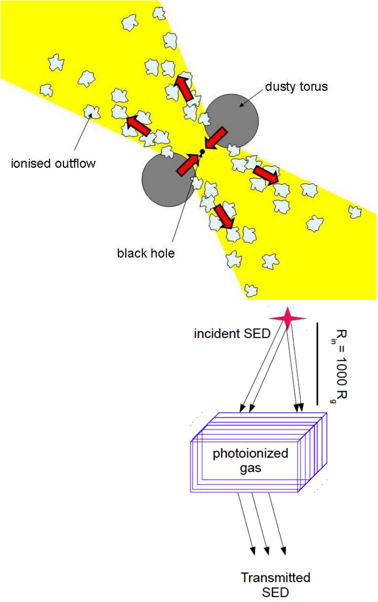

One photoionization component

1. parameters: A_i - Solar :), $R, n_0, N_{tot}, L_{ion}, SED, C_f = 1$
2. 1D non-LTE radiative transfer with ionization and thermal eq.: CLOUDY, XSTAR, TITAN, ION, PHASE, SPEX, XABS, SLAB
3. ionization parameter:

$$\xi_0 = \frac{L_{ion}}{n_0 R^2}$$

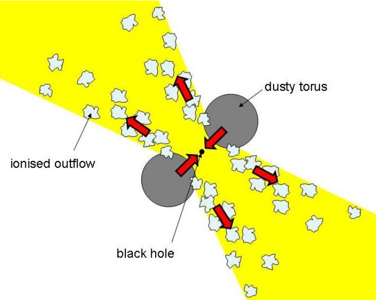

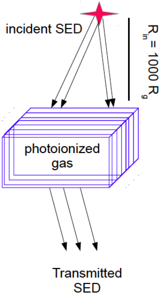

One photoionization component

1. parameters: A_i - Solar :), $R, n_0, N_{tot}, L_{ion}, SED, C_f = 1$
2. 1D non-LTE radiative transfer with ionization and thermal eq.: CLOUDY, XSTAR, TITAN, ION, PHASE, SPEX, XABS, SLAB
3. ionization parameter:

$$\xi_0 = \frac{L_{ion}}{n_0 R^2}$$

4. X-ray atomic data !!!
5. energy balance: $\Gamma_{bb} + \Gamma_{bf} + \Gamma_{ff} = \Lambda_{bb} + \Lambda_{bf} + \Lambda_{ff}$

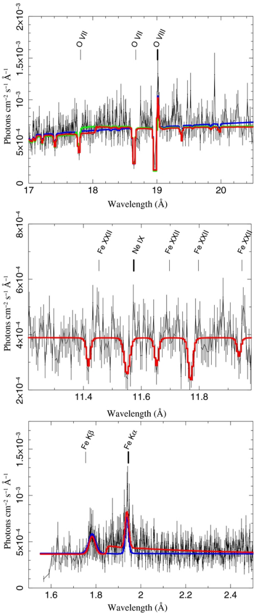

One photoionization component

1. continuity equation:
   $n = const$, $\xi = const$, $v = 0$
2. all codes - T, N_{tot}, ξ, EWs

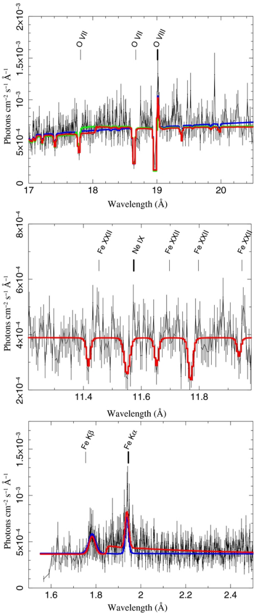

One photoionization component

1. continuity equation: $n = const$, $\xi = const$, $v = 0$
2. all codes - T, N_{tot}, ξ, EWs
3. location does not depend on gravity of the central BH

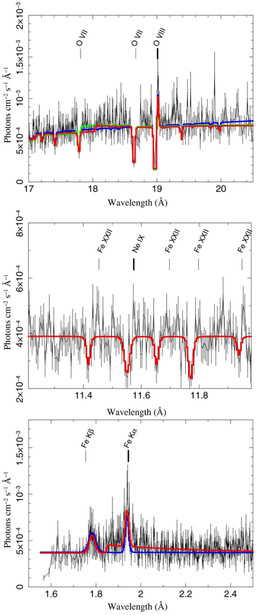

One photoionization component

1. continuity equation:
   $n = const$, $\xi = const$, $v = 0$
2. all codes - T, N_{tot}, ξ, EWs
3. location does not depend on gravity of the central BH
4. three components:
   $log(\xi) = 4.5, 3.3, 1.0$
   $v = -580, -450, -310$ km/s

NGC 4051, King + 10

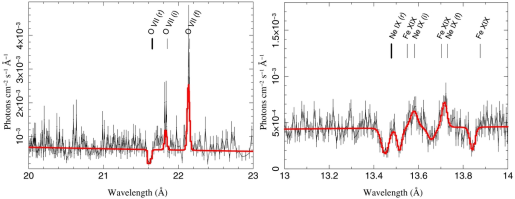

NGC 3783, Goncalves + 06
$\xi = 2500$, $N_{tot} = 4 \times 10^{22}$ cm^2, $v = 800$ km/s

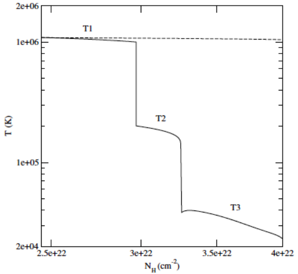

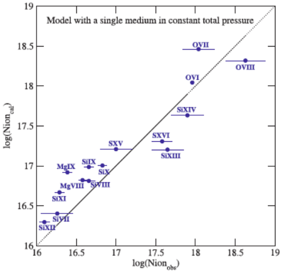

Continuous warm absorber

1. momentum equation: $P_{tot} = const$, $v = 0$
2. TITAN does this including calculation of $P_{rad}(\tau)$

NGC 3783, Goncalves + 06

$\xi = 2500$, $N_{tot} = 4 \times 10^{22}$ cm^2, $v = 800$ km/s

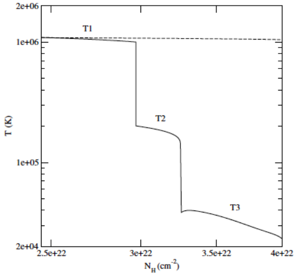

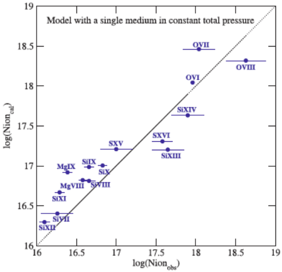

Continuous warm absorber

1. momentum equation: $P_{tot} = const$, $v = 0$
2. TITAN does this including calculation of $P_{rad}(\tau)$
3. $T(\tau), n(\tau), \xi(\tau), N_{tot}$, EWs
4. stability curve: T vs. Ξ

NGC 3783, Netzer + 03

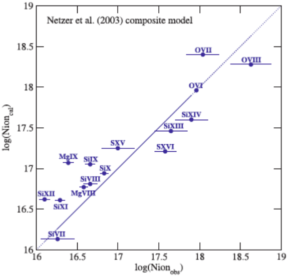

Dynamical ionization parameter

$$\Xi = \frac{\xi}{4\pi ckT} = \frac{L_{ion}}{4\pi cR^2}\frac{1}{nkT} = \frac{P_{rad}}{P_{gas}} = \frac{P_{rad}}{2.3\,P_{gas,H}},$$ Krolik + 1981

Hess + 1997, Stability curve,

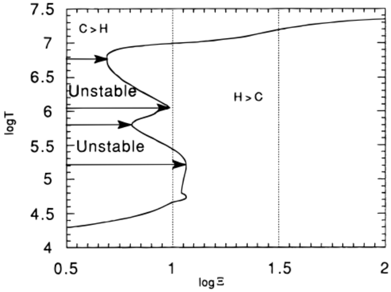

Dynamical ionization parameter

$$\Xi = \frac{\xi}{4\pi ckT} = \frac{L_{ion}}{4\pi cR^2}\frac{1}{nkT} = \frac{P_{rad}}{P_{gas}} = \frac{P_{rad}}{2.3\,P_{gas,H}},$$ Krolik + 1981

Hess + 1997, Stability curve, Influence of abundances

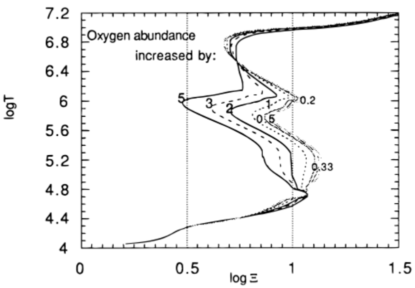

Stability curve

Chakravorty + 12, Different SEDs

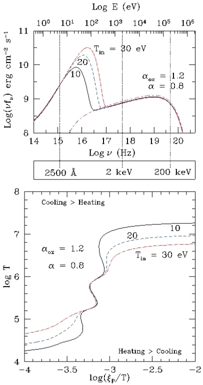

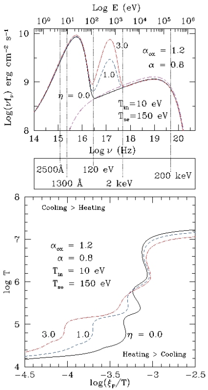

Stability curve

Chakravorty + 12, Different SEDs

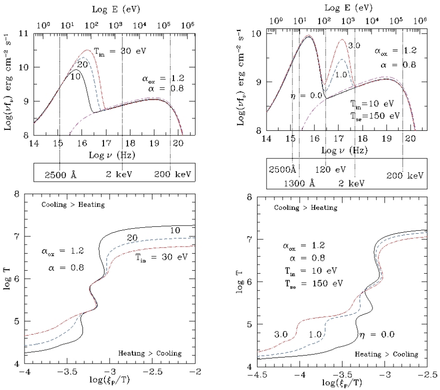

Różańska + 08

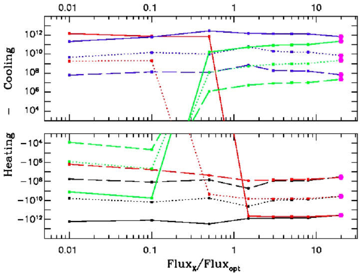

Net bound−free (Ion. − Rec.)
Net free−free (H − C)
Net Compton (H − C)
Net bound−bound (H − C) LINES

solid line - $n = 10^{10}$ cm^2
dotted line - $n = 10^{8}$ cm^2
dashed line - $n = 10^{6}$ cm^2

Stability curve

One constant density component has constant ξ, and it occurs as the one point on the stability curve:

NGC 3783, Krongold + 03

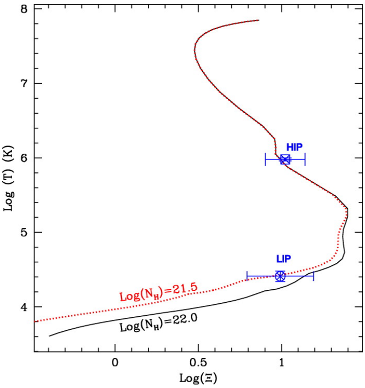

Stability curve

One constant density component has constant ξ, and it occurs as the one point on the stability curve:

NGC 5548, Steenbrugge + 05

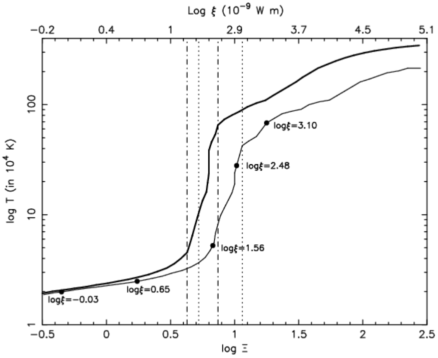

ESO 113-G010, Mehdipour + 12

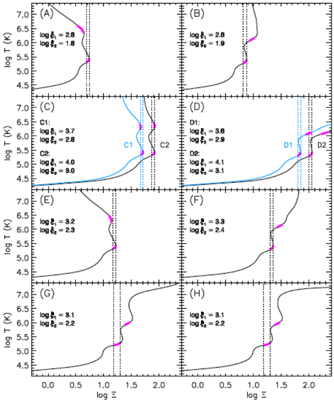

Stability curve

One constant density component has constant ξ, and it occurs as the one point on the stability curve:

$$\Xi = \frac{L_{ion}}{4\pi c R^2}\frac{1}{nkT} = \frac{P_{rad}}{P_{gas}}$$

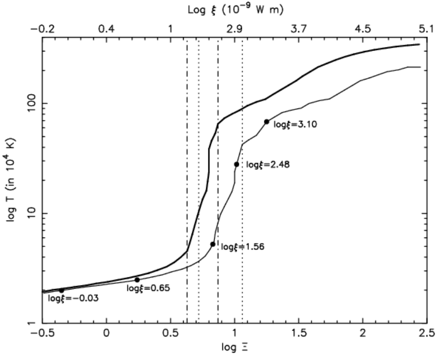

Stability curve

An absorber under constant total pressure, $P_{tot} = P_{rad} + P_{gas}$, solves the pressure structure: $P_{rad}(\tau)$ and $P_{gas}(\tau)$, and the whole stability curve is computed:

$$\Xi = \frac{P_{rad}(\tau)}{P_{gas}(\tau)}$$

HS 1603+3820
Różańska + 12

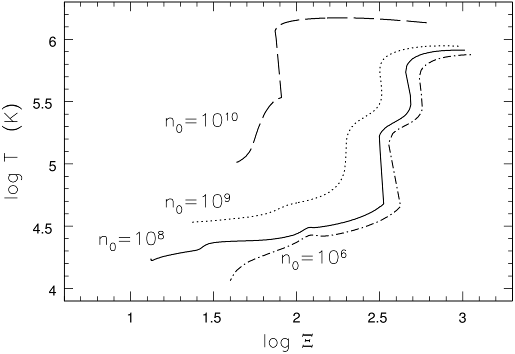

Equivalenth Hydrogen column densities, ion by ion

NGC 5548, Steenbrugge + 05

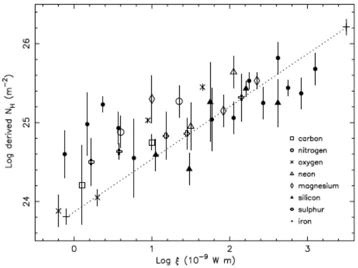

Fig. 11. The total hydrogen column density N_{H}, assuming solar abundances (Anders & Grevesse 1989) derived using Eq. (3), plotted versus ionization parameter. The ionic column densities were taken from Tables 4 and A.1 assuming a velocity broadening of 140 km s^{-1}. For clarity, no upper limits have been plotted. The best fit results for model D are plotted as the two crosses connected by a dotted line.

Mrk 273, Costantini + 07

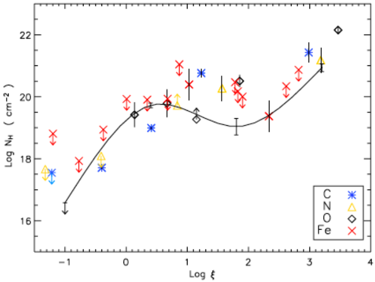

Fig. 10. The hydrogen column density as a function of the ionization parameter determined for: single ions (individual points) and an N_{H} continuous distribution model (solid line). See Sect. 2.4.2 for a full description.

Equivalenth Hydrogen column densities, ion by ion

Holczer + 07

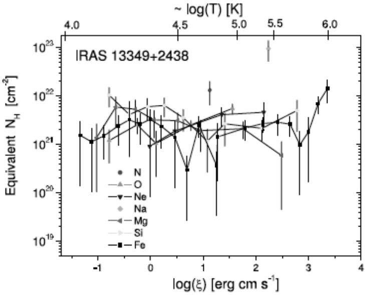

FIG. 4.—Equivalent N_H distribution (eq. [8]) obtained for the IRAS 13349+2438 outflow, assuming that ions form at ξ_{max} and assuming solar abundances (Asplund et al. 2005). Lines are drawn between data points to guide the eye. Vertical offsets between elements indicate deviations from solar abundances. The corresponding temperature scale obtained from the XSTAR computation is shown at the top of the figure. [*See the electronic edition of the Journal for a color version of this figure.*]

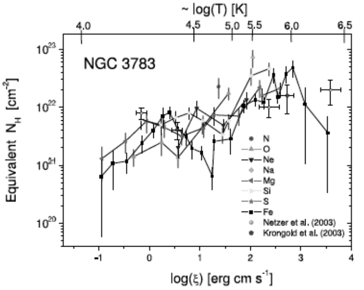

FIG. 6.—Equivalent N_H distribution (eq. [8]) obtained for the NGC 3783 outflow, assuming that ions form at ξ_{max} and assuming solar abundances (Asplund et al. 2005). Lines are drawn between data points to guide the eye. Vertical offsets between elements indicate deviations from solar abundances. The corresponding temperature scale obtained from the XSTAR computation is shown at the top of the figure. The Netzer et al. (2003) three-component model results and the Krongold et al. (2003) two-component model results are plotted for comparison. [*See the electronic edition of the Journal for a color version of this figure.*]

Structure of the warm absorber

AMD is: $\xi \frac{dN_H}{d\xi}$ vs. $\log(\xi)$

Holczer + 07

5. ABSORPTION MEASURE DISTRIBUTION

5.1. *Method*

The large range of ionization states present in the absorber strongly suggests that the absorption arises from gas that is distributed over a wide range of ionization parameters. The total hydrogen column density $N_{\rm H}$ along the line of sight can therefore be expressed as an integral over its distribution in $\log \xi$. We call this continuous distribution the absorption measure distribution (by analogy to the emission measure distribution in emission-line spectra):

$$\mathrm{AMD} = dN_{\rm H}/d(\log \xi), \tag{5}$$

$$N_{\rm H} = \int \mathrm{AMD}\, d(\log \xi). \tag{6}$$

The relation between the ionic column densities $N_{\rm ion}$ and the AMD is then expressed as

$$N_{\rm ion} = A_z \int \frac{dN_{\rm H}}{d(\log \xi)} f_{\rm ion}(\log \xi)\, d(\log \xi), \tag{7}$$

where $N_{\rm ion}$ is the measured ion column density, A_z is the element abundance with respect to hydrogen (assumed to be constant throughout the absorber), and $f_{\rm ion}(\log \xi)$ is the fractional ion abundance with respect to the total abundance of its element. Here we aim at recovering the AMD for IRAS 13349+2438.

As an initial approximation to be relaxed later, let us assume that each ion forms exclusively at the ionization parameter $\xi_{\rm max}$ where its fractional abundance peaks. Furthermore, if solar abundances $A_{Z_\odot}$ are assumed, the equivalent hydrogen column density can be calculated separately from each ion using the relation

$$N_{\rm H} \simeq \frac{N_{\rm ion}}{f_{\rm ion}(\xi_{\rm max}) A_{Z_\odot}} \tag{8}$$

and can be placed at the position of $\xi_{\rm max}$ on an $N_{\rm H}(\log \xi)$ plot. For this we employed the XSTAR code (Kallman & Krolik 1995) version 2.1kn3 to calculate $f_{\rm ion}(\log \xi)$ using the continuum derived in § 3.1, extrapolated to the range of 1–1000 ryd. The results for IRAS 13349+2438, using solar abundances from

Structure of the warm absorber

Absorption Measure Distribution - constant density

Holczer + 07

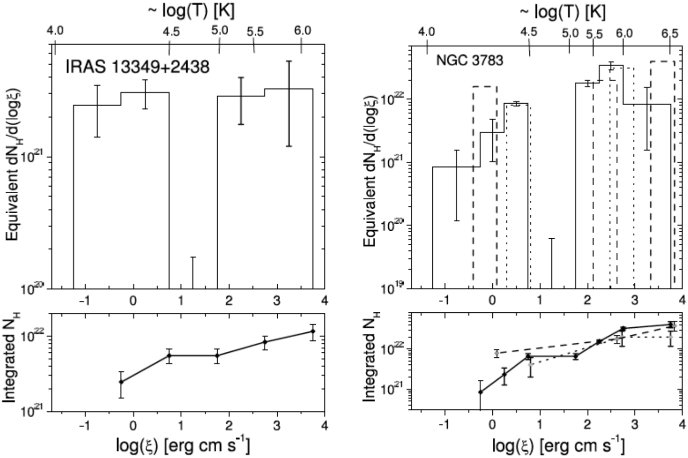

Observed AMD

Stern + 14

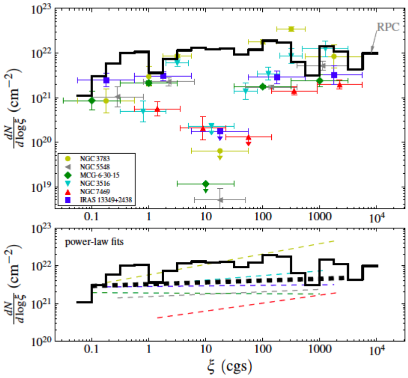

Behar + 09

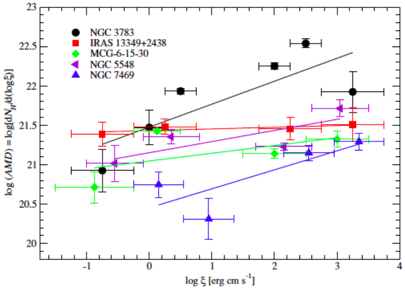

Observed AMD

Stern + 14

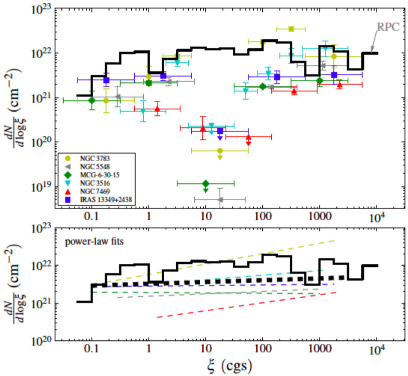

Rradiation Pressure Confinement

$$dP_{gas}(\tau) = P_{rad} e^{-\tau} d\tau$$

CLOUDY computations under constant pressure:

$$P_{gas}(\tau = 0) = const$$

Modelled AMD

Mrk 509, Adhikari + 15, submitted to ApJ

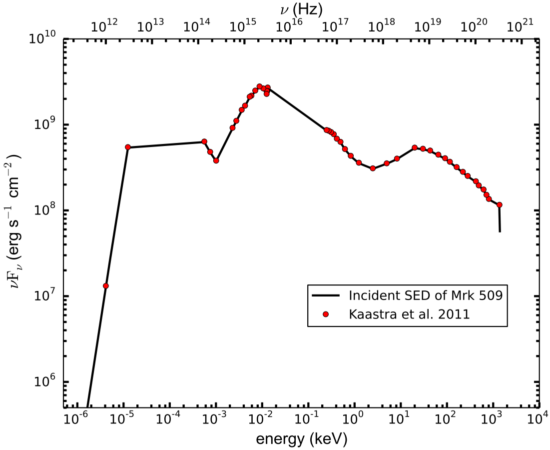

Modelled AMD

Stability curves computed by TITAN and CLOUDY

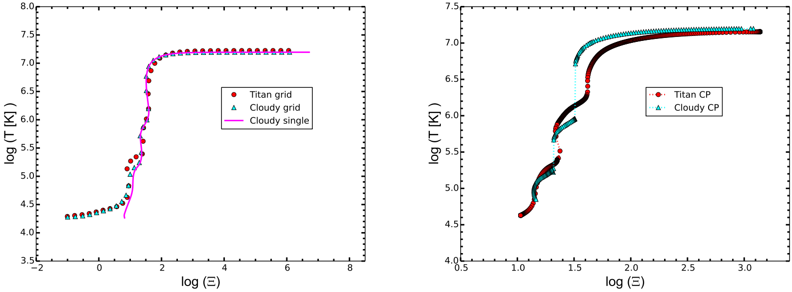

CLOUDY: $\Xi = \frac{L_{ion}}{4\pi c R^2} \frac{1}{nkT}$

Modelled AMD

Stability curves computed by TITAN and CLOUDY

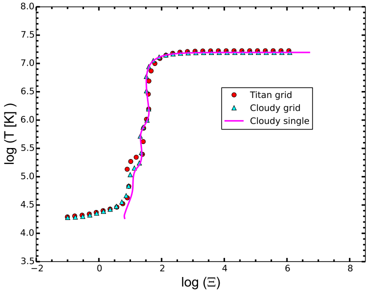

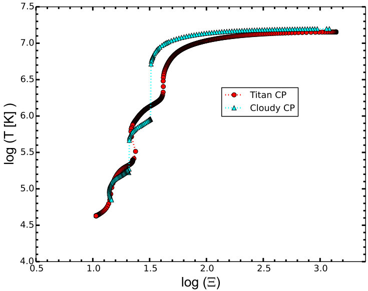

CLOUDY: $\Xi = \frac{L_{ion}}{4\pi c R^2} \frac{1}{nkT}$ TITAN: $\Xi = \frac{P_{rad}(\tau)}{P_{gas}(\tau)}$

Modelled AMD

Mrk509, Adhikari + 15, submitted to ApJ

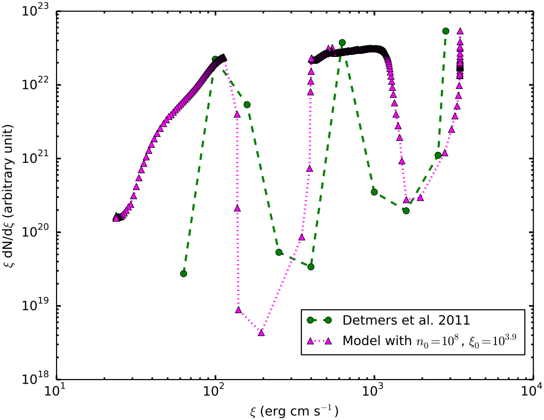

Modelled AMD

Stern + 14, Mean AGN SED

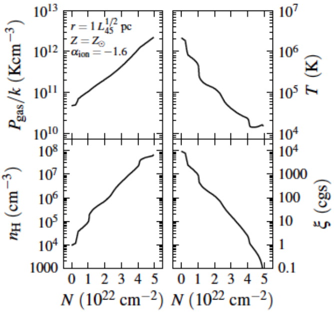

Adhikari + 15, SED for **Mrk 509**

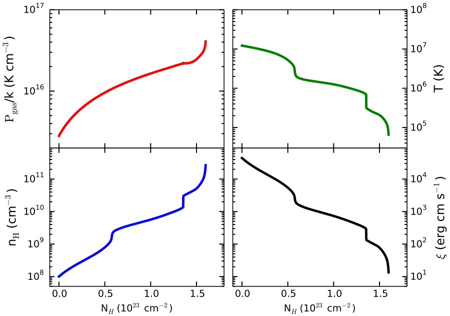

Radiation Pressure

Mrk509, Różańska + 08,
All clouds are dominated by radiation pressure

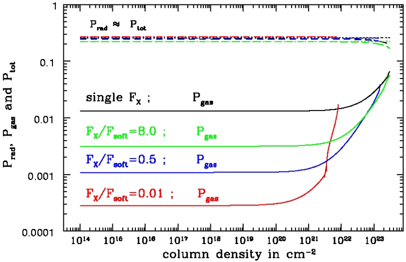

$n_0 = 10^6$ cm^{-3}, $\xi = 10^5$

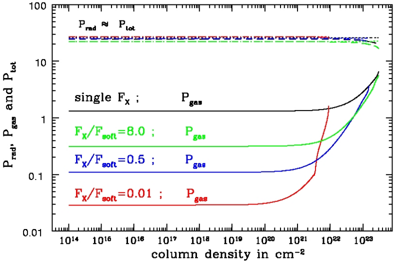

$n_0 = 10^8$ cm^{-3}, $\xi = 10^5$

Conclusions

1. Observed AMD are model dependent,

Conclusions

1. Observed AMD are model dependent,
2. Strong deeps in AMD can be explained as an evidence of thermal instability in case of Mrk 509,

Conclusions

1. Observed AMD are model dependent,
2. Strong deeps in AMD can be explained as an evidence of thermal instability in case of Mrk 509,
3. Modelled AMD agree with observations for the warm absorber being under constant total pressure,

Conclusions

1. Observed AMD are model dependent,
2. Strong deeps in AMD can be explained as an evidence of thermal instability in case of Mrk 509,
3. Modelled AMD agree with observations for the warm absorber being under constant total pressure,
4. TITAN code reproduces the structure of warm absorber, where ionization parameter is derived from the radiation pressure which decreases due to all absorption non-LTE processes,

Conclusions

1. Observed AMD are model dependent,
2. Strong deeps in AMD can be explained as an evidence of thermal instability in case of Mrk 509,
3. Modelled AMD agree with observations for the warm absorber being under constant total pressure,
4. TITAN code reproduces the structure of warm absorber, where ionization parameter is derived from the radiation pressure which decreases due to all absorption non-LTE processes,
5. To confirm our results we should consider other sources with known SEDs.

Summary

1. Absorption Measure Distribution give information about the warm absorber structure,

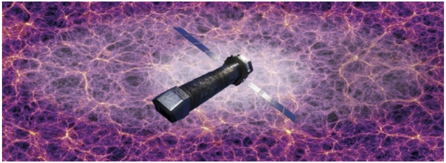

Summary

1. Absorption Measure Distribution give information about the warm absorber structure,
2. The measurement of elements content and ionization provides us with the distribution of metals in the Universe,

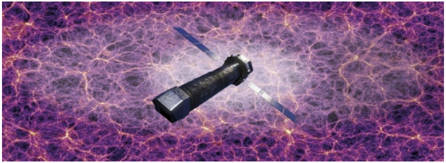

Summary

1. Absorption Measure Distribution give information about the warm absorber structure,
2. The measurement of elements content and ionization provides us with the distribution of metals in the Universe,
3. Higher resolution data allows us to detect more ionization species, which will complete the AMD.

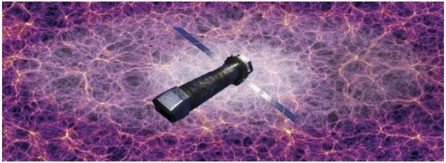

ATHENA X-ray observatory

X-IFU - X-ray Integral Field Unit, $\Delta E = 2.5$ eV @ 1 keV
WFI - Wide Field Imager , $\Delta E = 150$ eV @ 6 keV

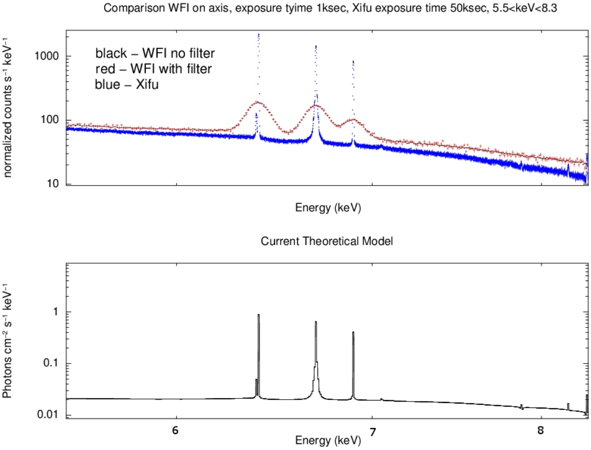

ATHENA X-ray observatory

Our best fitted AMD model with high energy resolution

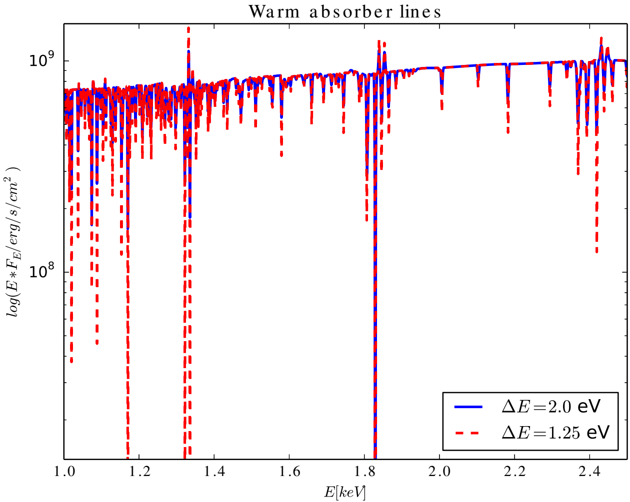

ATHENA X-ray observatory

Our best fitted AMD model with high energy resolution

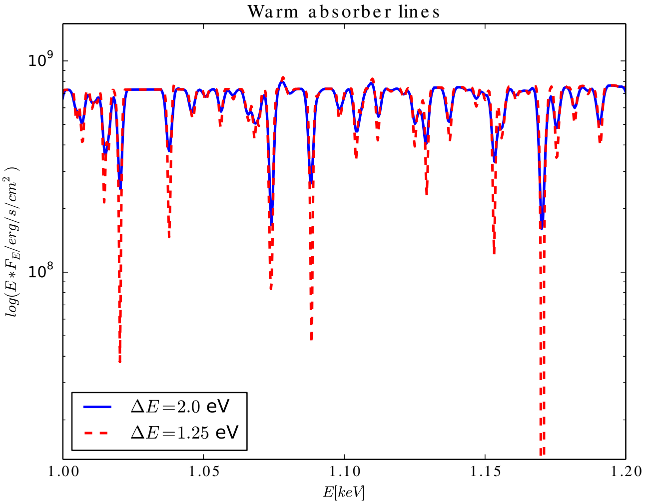

ATHENA X-ray observatory

Our best fitted AMD model with high energy resolution